This is a peer-reviewed, accepted author manuscript of the following conference paper: Amiolemen, A, Fusiek, G & Niewczas, P 2024, Towards the development of a photonic current sensor for HVDC networks. in 2024 IEEE International Instrumentation and Measurement Technology Conference (I2MTC). IEEE, Piscataway, NJ

Towards the Development of a Photonic Current Sensor for HVDC Networks

Alfred Amiolemen
Department of Electrical and Electronic Engineering
University of Strathclyde

Grzegorz Fusiek
Department of Electrical and Electronic Engineering
University of Strathclyde

Pawel Niewczas
Department of Electrical and Electronic Engineering
University of Strathclyde

***Abstract*— This article introduces an innovative optical current sensor (OCS) that integrates photonic and piezoelectric technologies to facilitate the distributed measurement of current within High Voltage Direct Current (HVDC) networks. The proposed sensor is designed to fit in an HVDC subsea cable splice to provide remote, distributed current measurement for enhanced monitoring and protection of HVDC power cable assets. The prototype transducer comprises a non-linear amplifier with an enhanced dynamic range to reduce the measurement errors that are dominated by the limitations of the sensor interrogation system at low input signal levels. The development and testing procedures were carried out within a controlled laboratory setting, adhering to the accuracy specifications stipulated by the IEC 61869-14 standard.**

Keywords—Optical current sensor (OCS), Low voltage transducer (LVT), High Voltage Direct Current (HVDC), Direct Current Current Transformer (DCCT)

I. INTRODUCTION

The evolving energy landscape is marked by a shift towards decarbonization in electricity generation and utilization. This shift has led to a diverse and complex mix of deterministic and stochastic, synchronous, and asynchronous energy sources. Many of these generation assets are located in remote and challenging environments. Consequently, integrating their generated power through a common transmission corridor becomes crucial to achieving improved power flow density and efficiency from varied sources. High Voltage Direct Current (HVDC) technology plays a vital role in evacuating the generated power due to its capacity for sources integration, minimizing losses, increased energy density, enhancing power control, controllability, and stability, while maintaining lower costs. Ensuring the protection of these assets is essential to meet the minimum reliability, availability, and constant voltage requirements expected for power flow from generation to utilisation [1]-[3].

In HVDC systems, traditional methods for measuring current and voltage are employed. Shunt and magnetic based sensors like fluxgate and Hall effect are the prevalent choices in the industry for current measurement in DC net

works. This preference arises from the fact that DC lacks a changing magnetic field and zero-crossing, which renders common AC-based magnetic sensors unsuitable. However, it's important to note that magnetic-based sensors for DC current measurement also have certain limitations, particularly regarding saturation and operational restrictions imposed by their Curie thermal range [4]-[7], notwithstanding the difficulty of remote interrogation and multiplexing.

Sensors utilizing fibre Bragg gratings (FBGs) in combination with giant magnetostrictive materials (GMM), such as Terfanol-D have been proposed; they exhibit potential for remote interrogation and multiplexing. Nevertheless, these sensors are vulnerable to issues of nonlinearity, saturation, and temperature dependency which adversely impact measurement accuracy. Fiber-optic current sensors (FOCSs) relying on the Faraday effect offer the potential for achieving high measurement accuracy (as low as 0.1%). However, they are susceptible to environmental vulnerabilities, especially when used over long distances. Lumiker's OCS technology, also based on the Faraday effect, addresses these vulnerabilities but introduces complexity in the optical system, particularly when multiplexing is required [8].

This paper introduces an innovative optical current sensing approach as an alternative to existing methods, featuring a shunt as the primary sensing element. In this Optical Current Sensor (OCS), the electrical signal from the shunt is modulated by an optical carrier wave. This system integrates electrical signal conditioning circuitry with a low-voltage transducer employing piezoelectric and photonic principles. The sensor is entirely passive, self-sustaining, immune to electromagnetic interference, and can be multiplexed. Each crucial component underwent individual characterization in a laboratory setting to ensure compliance with IEC 61869-14 standards, for DC current transformer (DCCT).

II. MEASUREMENT SPECIFICATION

A. Specification

The proposed OCS is expected to measure a nominal current of 1 kA, although current in HVDC lines can range from below that nominal to several kA above the nominal [9], [10], depending on the thermal and insulation capacity of the lines. Nonetheless, the current flowing in these conductors can deviate from this nominal value, depending on the loading and transients' condition of the line, and the sensor is expected to measure accurately the condition of the line within its designed capability.

The K_{pcr} and K_{ALF} factors are the rated extended primary current factor and the accuracy limit factor, respectively, as stipulated by IEC 61869-14. The standard values of K_{ALF} are 3, 6, 10, and 20 [11].

III. OPTICALCURRENT SENSOR

A. Sensor Concept.

The sensor operation requires a voltage drop in a shunt. The present configuration is capable of producing a 50 mV voltage drop at nominal current. The electrical power associated with this voltage drop is harvested by a dedicated harvester to drive a signal conditioning circuit. The signal from the amplifier drives a low-voltage transducer which is composed of a piezoelectric (PZT) transducer and FBG housed in a hermetically sealed butterfly package with Kovar pins terminals for connection. Fig. 1 depicts a circuit comprising three crucial components amongst others: an energy harvester, an amplifier, and an LVT (Low-Voltage

Transducer). These components collectively handle the circuit's driving and signal manipulation from the primary shunt source. Meanwhile, the interrogator's role is to detect the peak wavelength change in FBG spectrum and transmit data for subsequent analysis.

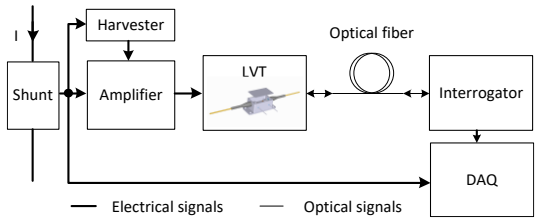

Fig. 1HVDC Sensor Concept

The circuit operates with extremely low power consumption, in the micro-watt range. Consequently, meticulous component selection is imperative, focusing on micro-power-rated components to align with the circuit's stringent power budget constraints.

B. Shunt

The selection of a shunt resistor as the primary sensing element was made due to its capacity to operate dynamically across a wide range and its accuracy in converting current into an equivalent voltage span, even when subjected to a broad thermal and frequency operating conditions. The mathematical model for the voltage variations across the shunt can be expressed with the relationship below [12].

For an AC signal, the voltage drop is:

$$V_{drop} = L\left(\frac{di}{dt}\right) + Ri \tag{1}$$

For DC signal, the voltage drop is:

$$V_{drop} = IR \tag{2}$$

The shunt thermal resistance behaviour under a thermal stress which can be due to self-heating and ambient temperature, can be mathematically represented by this relationship [7]:

$$R_T = R_A(1 + \alpha_{TK}(T - T_A)) = R_A(1 + \alpha_{TK}(\Delta T) \tag{3}$$

$$\Delta T = T_{selfheating} + T_{ambient} \tag{4}$$

where: α_{TK} is the temperature coefficient, R_T is the present resistance, R_A is the ambient resistance, T is the present temperature and T_A is the ambient temperature.

The self-heating effect of the shunt is due to the Joule heating of the shunt element which can be related with the following expression.

$$P_{Loss} = R(T)I^2 \tag{5}$$

$$T_{selfheating} = R_{th,total}P_{Loss} = R_{th,total}(R(T)I^2) \tag{6}$$

Taking *R(T)* as the total resistance, assuming the total resistance does not differ significantly from the ambient resistance and substituting into eqn. 3

$$R(I, \Delta T_{amb}) = R_o(1 + \alpha_{TK}\Delta T_{amb} + \alpha_{TK}R_{th,total}R_A I^2) \tag{7}$$

The voltage drop over the resistor with the heating condition is given by

$$U_{shunt} = R(I, \Delta T_{amb})I = R_A(1 + \alpha_{Tk}\Delta T_{amb})I + \left(\alpha_{TK}R_{th,total}R_A^2\right)I^3 \tag{8}$$

The relationship underlining a shunt under thermal stress due to Joule heating is expressed by a 3rd degree polynomial. Taking a look at the polynomial equation, there will be deviation from the nominal voltage even at the same current amplitude due to thermal heating. At that point, the voltage drop will increase from the nominal 50 mV which it was designed for. For the energy harvester and precision amplifier details, refer to [13].

C. Low Voltage Transducer (LVT)

The LVT consists of a combination of a PZT constructed using a PICMA® stack manufactured by Physik Instrumente and an FBG. The FBG sensor is inscribed within a single-mode optical fibre, which is suspended across the PZT element. This entire assembly is enclosed in a hermetically sealed butterfly package conforming to industry standards, with the PZT stack being powered via two Kovar pins.

The LVT serves as a two-tier transduction unit, where the initial transformation involves voltage being converted into mechanical strain within the PZT. Subsequently, this mechanical strain is transduced into variations in the grating pitch and refractive index within the FBG, facilitating precise and integrated measurement capabilities. The sensor and its functional principle are illustrated in Fig 2 and 3 below.

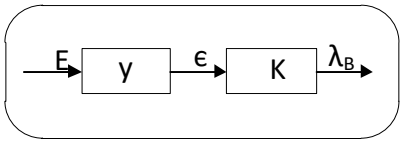

Fig. 2 LVT Functional Process Flow. E, voltage; y, voltage-to-strain transduction; ε, strain; K, strain-to-wavelength transduction; λ_B, FBG center wavelength.

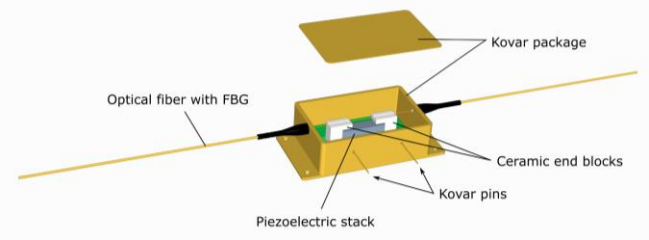

Fig. 3 LVT Transducer

E is the external electric field, y is the PZT transfer function, having ε as strain (length deformation) which is the output of y block, while K is the FBG transfer function having λ_B (FBG Centre Wavelength) as output [14].

$$y = Md_{xy} \tag{9}$$

$$\varepsilon = Md_{xy}E \tag{10}$$

$$\frac{\Delta l}{l} = \frac{Md_{xy}V}{l} \tag{11}$$

$$\Delta l = Md_{xy}V \tag{12}$$

where d_{xy} is the PZT strain coefficient. Note that different crystalline quartz material symbolised by the subscript $_{xy}$ have different properties. Δl is the change in length and V is the applied voltage. M is the strain amplification coefficient.

$$\lambda_B = \epsilon K \quad (13)$$

For a single mode fibre (SMF28), the change in wavelength ratio can be mathematically modelled [15]:

$$\frac{\Delta\lambda}{\lambda} = 0.79\varepsilon \quad (14)$$

$$K = 2n_{eff}\Lambda \quad (15)$$

$$\lambda_B = Md_{xy}E(2n_{eff}\Lambda) \quad (16)$$

$$= \varepsilon(2n_{eff}\Lambda)$$

where 0.79 is the photo elastic coefficient linking wavelength change and strain for a single-mode fibre. As shown in the Fig. 2 and 3, under the influence of external electric field, the PZT element reacts through shape deformation which manifests as strain. The strain is transferred to the FBG which responds by a shift in Bragg wavelength. The Bragg wavelength change is then evaluated by an interrogator. In the final analysis, the LVT quantifies voltage (V) in Bragg wavelength shift (pm).

IV. EXPERIMENTS AND RESULTS

A. LVT Characterisation

The LVT was subjected to a characterization process to ascertain its response to the input signal. This involved feeding the amplified signal from the operational amplifier (op-amp) into the Kovar pin terminals of the LVT component. The characterization was conducted by cyclically applying voltage ramps of 1 V, 3 V, and 5 V. It was observed that this measurement cycle exhibited a hysteresis loop, a common trait seen in materials with charge retention capabilities.

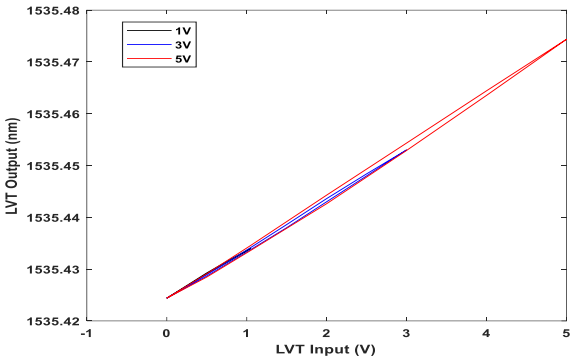

Fig. 4 Hysteresis Analysis of the LVT

Primarily capacitive in nature, the LVT's hysteresis behaviour creating this displacement is attributed to the unsymmetrical charge polarisation between the forward and reverse paths at the same voltage levels. This discrepancy which is due to alterations in strain polarization balance is influenced by an external field. Consequently, the counterbalance results in a displacement, which manifests as hysteresis [16], [17]. The introduction of a curve fitting algorithm to both top and bottom hysteresis parts can rectify this issue to some extent, albite introducing a corresponding measurement error. For the linear amplification characterisation of the amplifier and for harvester characterisation refer to [13].

B. Response to Transient Edge

The circuit's transient response to changes in stability of the signal magnitude and rise time is a critical consideration. An experiment was conducted to assess the circuit's behaviour under this input condition, specifically emulating a 1 ms rising edge of a potential power network fault current.

The experiment successfully captured the salient characteristics of the transient response, as depicted in Fig. 5. During the transient, the circuit drove the amplifier into a saturation mode, resulting in signal clipping at approximately 3.3 V. This value corresponds to both the accuracy limit of the sensor (known as K_{ALF}) and the upper rail limit of the sensor due to output point settings within the energy harvester circuit.

This experiment highlights the alignment between the LVT signal and the optical signal, indicating a promising capability for this optical current sensor to capture crucial transient moments during practical deployment for measurement purposes.

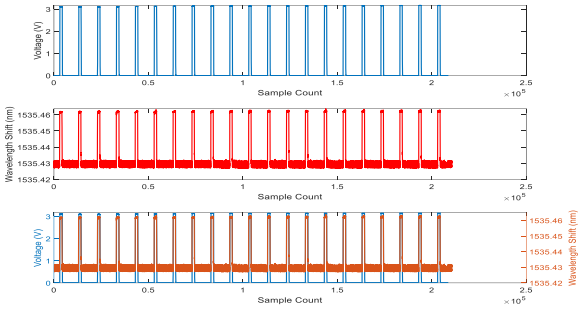

Fig. 5. Circuit Response to Transient Condition

V. CONCEPT OF AN HVDC CABLE SPLICE SENSOR

The target application for the proposed DC sensor is within an HVDC cable splice enclosure. Fig. 6 illustrates the concept of the shunt arrangement, made of Manganin, that would be included in the cable splice enclosure. Manganin has a low temperature coefficient of resistivity (1 × 10−5/°C), making it suitable for a precision shunt resistor. The conductor that is being spliced would terminate on either side of the shunt. The central narrowing of the cylinder constitutes a 50 μΩ resistance that will produce a 50 mV voltage drop at the nominal current of 1000 A flowing through the conductor. The LVT, the energy harvester and amplifier are proposed to be housed next to the central narrowing of the shunt arrangement. Since the conductor is at high voltage potential, and the shunt arrangement will be surrounded by a sheath at ground potential, it is imperative to shield the vulnerable electronics with a form of a Faraday cage. This structure, as depicted in Fig. 6 is galvanically connected to one side of the shunt cable termination but is isolated from the other side (End A) to prevent an additional conduction path outside of the shunt narrowing section.

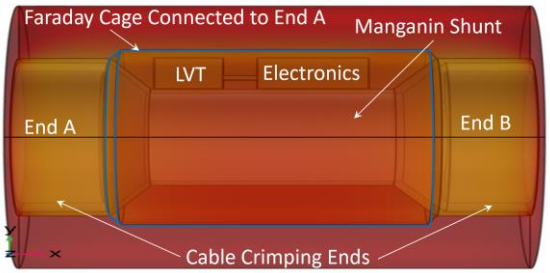

Fig. 6 A representation of the shunt and sensor assembly

VI. MEASUREMENT ACCURACY

Accurate measurement is of paramount importance in comprehending the limitations of any process and system. In the context of this specific application, standards defined by IEC 61869-14 dictate a maximum allowable error of 5%.

The analysis of the measurements conducted so far has revealed that systematic errors tend to affect smaller, borderline signal values more significantly than larger ones. Specifically, from the measurement analysis, a 1 pm wavelength change corresponds to an approximate voltage deviation of 4.8 mV. This information underscores the need to account for and mitigate errors in the measurement process to ensure accuracy, particularly when dealing with lower signal values. It's important to note that the accuracy limitation of the FBG interrogation system used in this research is specified within a range of 1-3 pm wavelength change. To achieve an accuracy that meets the required specifications for the IEC 61869-14 standard of maximum 5% error, an interrogator that is 1/14th of the accuracy level of the current interrogator will be required. Iinterrogators with that level of accuracy are available commercially. For example, according to FAZT INTERROGATOR technical specification [18], it has a repeatability of < 0.05 pm, that translate to providing an accuracy that is 20 times better than the current interrogator.

A. Op-Amp Modification

The selection of an LVT with a nominal voltage of 1 V imposes an amplification requirement for the input signal originating from the shunt, which is inherently weak and lacks the capability to adequately drive the LVT. To address this, an operational amplifier in a non-inverting configuration was originally employed to achieve the necessary signal amplification [13].

To improve the accuracy of the measurement, which is currently dominated by the interrogator limitations, the use of a non-linear amplifier to drive the LVT is proposed in this paper. It is proposed that signals are amplified at a greater proportion at low input voltage using a non-linear amplifier to artificially expand the measurement range. This approach would boost the low-level signals to the level where the interrogator error becomes less significant. Conversely, the high-level input signals would be compressed to maintain the overall input voltage range. The proposed amplification profile exhibits “dynamic sensitivity”, effectively elevating low voltage signals beyond the wavelength detection limitation of the current interrogator. The accompanying circuit configuration is depicted in Fig. 7.

The circuit transfer function can be expressed as follows:

$$V_{in} = V_{out}\left[\left[\frac{R_b}{R_b+R_{f1}}\right]+\left[\frac{R_b}{R_b+R_{f2}}\right]+\left[\frac{R_b}{R_b+R_{f3}}\right]\right] \quad (17)$$

$$V_{in} = V_{out}\left[\frac{R_b}{R_b+R_f}\right]+(V_{out}-V_{f1})\left[\frac{R_b}{R_b+R_{f2}}\right]+(V_{out}-V_{f2})\left[\frac{R_b}{R_b+R_{f3}}\right] \quad (18)$$

$$\frac{V_{out}}{V_{in}} = \frac{1+\frac{V_{f1}N+V_{f2}P}{V_{in}}}{M+N+P} \quad (19)$$

where

$$M=\left[\frac{R_b}{R_b+R_{f1}}\right], N=\left[\frac{R_b}{R_b+R_{f2}}\right], P=\left[\frac{R_b}{R_b+R_{f3}}\right]$$

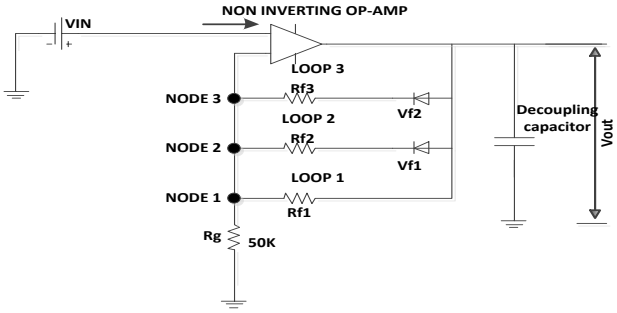

Fig. 7 Non-Linear Op Amp Circuit Configuration

There was a close alignment between the simulated, calculated and the experimental result of the Non-Linear configuration from Fig. 7 in Fig. 9.

B. Amplifier Characterisation

In order to ensure that the non-linear amplifier can effectively respond to variations in the transduced voltage level, it underwent characterization across a range of supply voltages, VCC (Voltage Common Collector), spanning from 1.5 V to 5 V. The emulated shunt signal was provided to the input of the amplifier, and the output response was observed. The results indicate that the signals were faithfully reproduced, effectively capturing the input signal until reaching the saturation limits. Note the greater gain of the amplifier for very low signals.

In Fig. 9, a comparative analysis was conducted between the *linear* and *non-linear* amplifier responses. The non-linear amplifier exhibited a distinctive behavior characterized by a sharp amplification of very low voltage inputs and a concurrent compression in amplification for inputs approaching nominal values and beyond.

This unique response pattern results in an extended operational range, making the non-linear amplifier suitable for a broader range of input voltages in contrast to the conventional amplifier.

With the accuracy limit within the IEC 61869-14 standard as the key driver of this solution, analysis was performed, comparing reconstructed voltage and reference voltage. Although the reconstructed voltage is yet to meet the standard in terms of accuracy limits requirements, there has been improvement in accuracy compared to the linear amplifier. A 1st order polynomial transfer function from the fitting was used to reconstruct the voltage from the wavelength for the

linear amplifier and a 2nd order polynomial for the Non-linear amplifier. Fig. 10Fig. 10 shows the error plot for linear and non-linear reconstructed voltage for comparison, showing a reduced error, particularly at low input voltage. Still, the present system is unable to meet the accuracy specifications provided by the IEC 61869-14 standard. This task will require an amplifier with still greater nonlinearity for low signals and/or more precise FBG interrogator. Furthermore, the error introduced by the hysteresis width will also need to be considered in the future investigations aimed at the reduction of the overall measurement error.

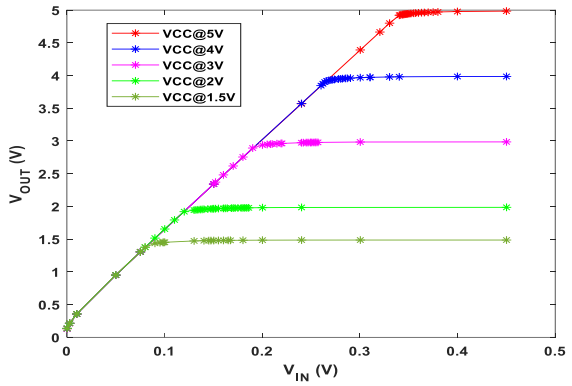

Fig. 8 Non-Linear Op-Amp Characterization

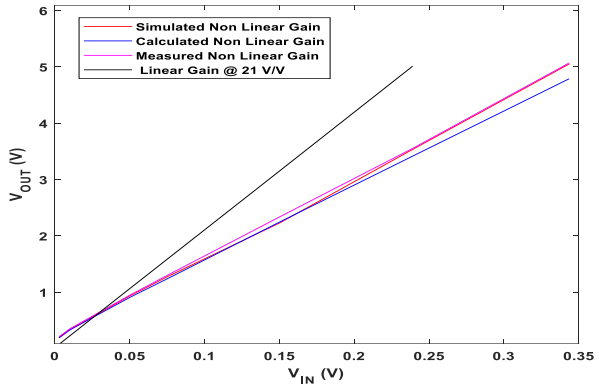

Fig. 9 Simulated, Calculated and experimented Op-amp response

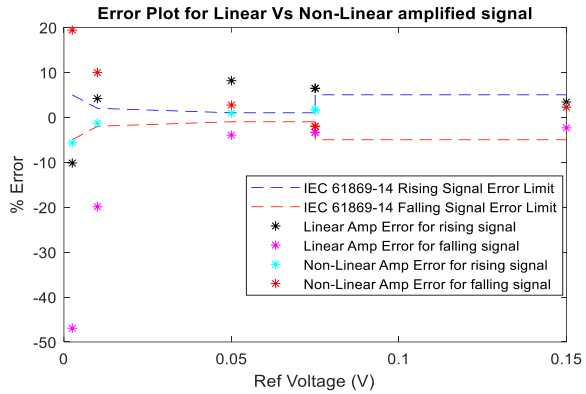

Fig. 10 Error plot for the reconstructed voltage from the linear vs non-linear gain amplifiers and the IEC 61869-14 accuracy specifications.

VII. CONCLUSION

In this study, a hybrid optical sensor was proposed for the measurement of current within an HVDC cable splice to facilitate distributed measurements for enhanced system monitoring and protection. The sensor, when fully developed, can be installed in multiple splice joints, piggybacking on the optical fiber cables installed in most transmission cables as signal transmission media.

To address concerns pertaining to measurement accuracy, a signal conditioning technique was proposed and demonstrated. The technique involves the use of nonlinear amplification of signals, effectively magnifying low-level signals and elevating them beyond the measurement device's error threshold. Notably, this solution is relevant due to its minimal power requirements and the absence of an additional circuit for gain selection based on input signal characteristics.

While the realization of the IEC 61869-14 standard remains an ongoing effort, the obtained results exhibit increasing promise. Anticipated improvements in both circuitry, equipment and measurement methodologies hold the prospect of aligning with the standard in due course.

REFERENCES

[1] M. Barnes, D. van Hertem, S. P. Teeuwsen, and M. Callavik, “HVDC Systems in Smart Grids,” 2017.
[2] ABB, “ABB review, HVDC special report,” 2014.
[3] SP Networks, “ANGLE-DC 2015 Electricity Network Innovation Competition,” 2015.
[4] M. A. Paun, J. M. Sallese, and M. Kayal, “Hall effect sensors design, integration and behavior analysis,” *Journal of Sensor and Actuator Networks*, vol. 2, no. 1, pp. 85–97, Mar. 2013, doi: 10.3390/jsan2010085.
[5] TI, “Introduction to Hall-Effect Sensors,” 2023. [Online]. Available: www.ti.com
[6] K. Maniar, “Comparing Shunt-and Hall-Based Isolated Current-Sensing Solutions in HEV/EV,” 2023. [Online]. Available: www.ti.com
[7] P. Weßkamp and J. Melbert, “3.4.4 - High Performance Current Measurement with Low-Cost Shunts by means of Dynamic Error Correction,” AMA Service GmbH, Dec. 2020, pp. 224–230. doi: 10.5162/sensoren2016/3.4.4.
[8] https://www.lumiker.com/en/camos200-current-monitoring/ (accessed on 14 June 2023)., “CAMOS200 Current Monitoring.”
[9] Scottish and Southern Electricity Network, “HVDC Technology Capability,” 2018. [Online]. Available: www.ssen.co.uk
[10] Dirk Van Hartem, Oriol Gommis-Bellmunt, and Jun Liang, *HVDC GRIDS*. IEEE PRESS, 2018.
[11] SASO IEC 61869-14, “INSTRUMENT TRANSFORMERS-Part 14: Additional requirements for current transformers for DC applications (SASO),” 2019.
[12] Pawel Piekielny and Andrzej Waindok, “Using Current shunt for the Purpose of High-Current Pulse Measurement,” *MPDI*, pp. 2–4, 2021, doi: 10.3390/s21051835.
[13] A. Amiolemen, G. Fusiek, and P. Niewczas, “Self-Powered Signal Conditioning Circuit for an HVDC Optical Current Sensor,” *IEEE Sens Lett*, pp. 1–4, Sep. 2023, doi: 10.1109/lsens.2023.3311676.
[14] R. Pallás-Areny and J. G. Webster, *Sensors and signal conditioning*, 2nd ed. Wiley, 2001.
[15] C. E. Campanella, A. Cuccovillo, C. Campanella, A. Yurt, and V. M. N. Passaro, “Fibre Bragg Grating based strain sensors: Review of technology and applications,” *Sensors (Switzerland)*, vol. 18, no. 9. MDPI AG, Sep. 15, 2018. doi: 10.3390/s18093115.
[16] Jinqiang Gan and Xianmin Zhang, “A review of nonlinear hysteresis modeling and control of piezoelectric actuators,” *AIP*, pp. 1–5.
[17] H Li, Y Xu, M Shao, L Guo, and D An, “Analysis for hysteresis of piezoelectric actuator based on microscopic mechanism,” *IOP*, pp. 1–6, 2018.
[18] FAZT, “FAZT I4-16 INTERROGATORS.” [Online]. Available: www.femtosensing.com